

Correlating Pit Initiation in Aluminum with Passive Oxide Defect Structure

K.R. Zavadil and P. Lu
Sandia National Laboratories
Albuquerque, NM 87185-0888

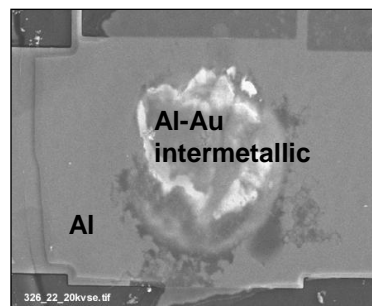
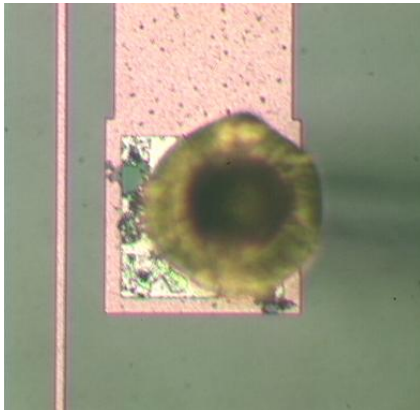
Acknowledgements: J. Soltis, Quest Integrity Group

DOE Basic Energy Sciences Office of Materials & Engineering Sciences

Sandia is a multiprogram laboratory operated by Sandia Corporation, a Lockheed Martin Company, for the U.S. Department of Energy's National Nuclear Security Administration under contract DE-AC04-94AL85000

Why study pit initiation in Aluminum?

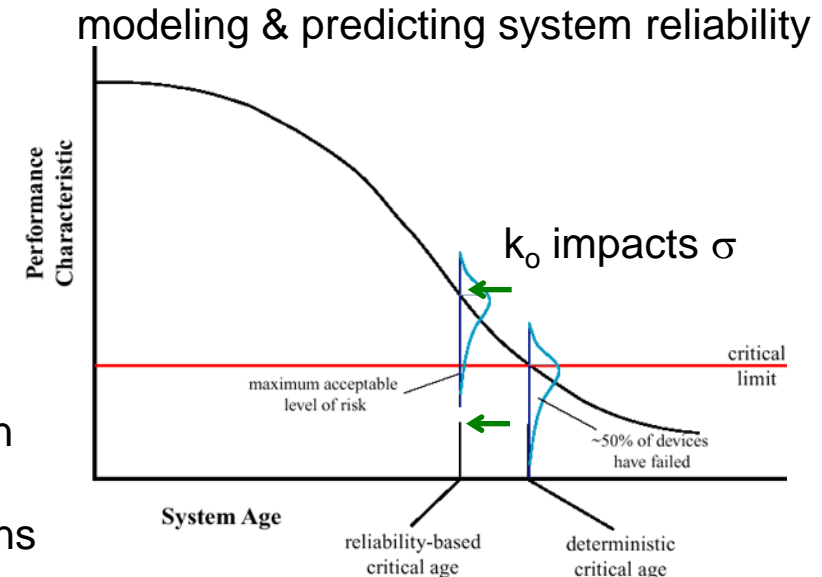
High consequence systems: minimal separation between initiation and damage
microelectronics – nanomaterials integration



Al interconnects can undergo galvanic corrosion

rate constant (k_o) - lump sum term for unknowns

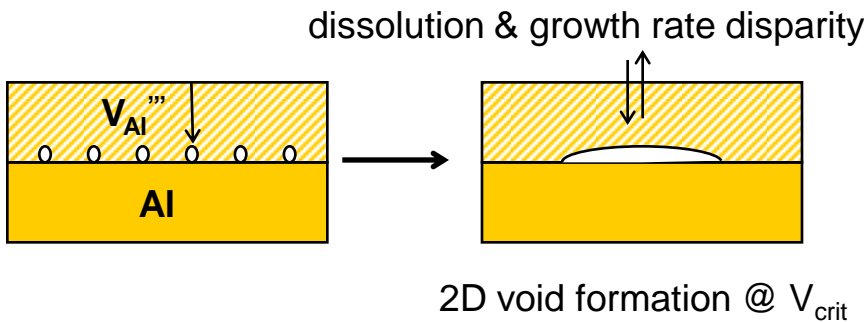
$$\frac{d(\Delta R / R_o)}{dt} = I(\text{defects}) k_o P_{Cl_2}(t) \left\{ 1 - \exp \left[- \left(\frac{H(t)}{\eta} \right)^\beta \right] \right\} \exp \left[- \frac{E_a}{RT(t)} \right]$$



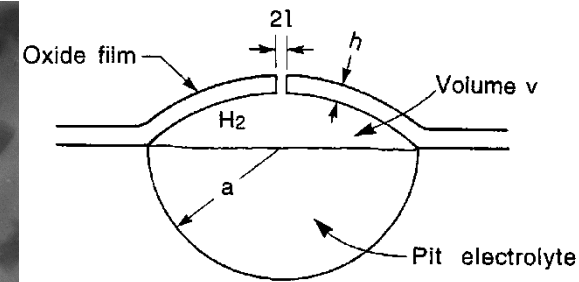
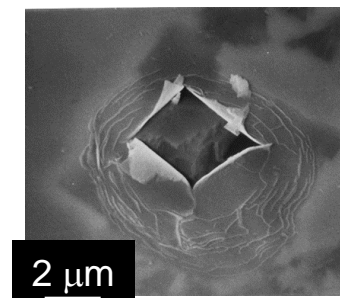
Reliability prediction requires relevant physical & chemical inputs of localized corrosion mechanisms

Proposed mechanisms for pit initiation

Vacancy condensation - Point Defect Model (Macdonald)

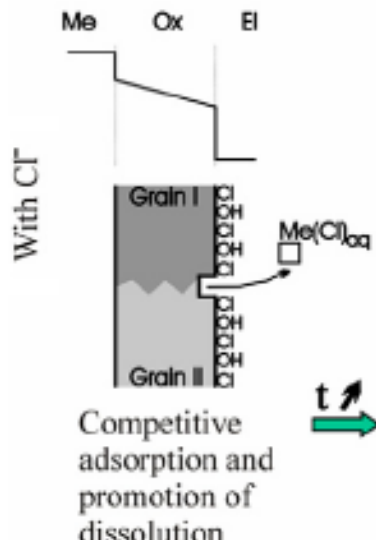


Nano-corrosion cells - Electrokinetic Model (McCafferty)

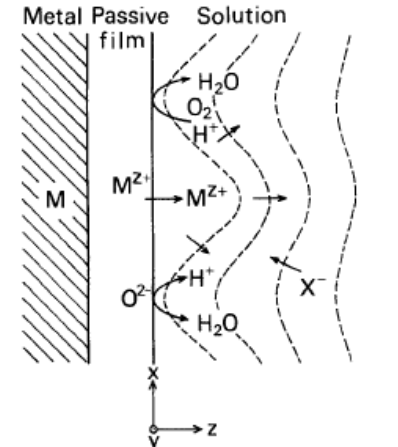


McCafferty & Natishan, 218th ECS #1322

Oxide grain boundaries - Marcus, Maurice & Strehbow



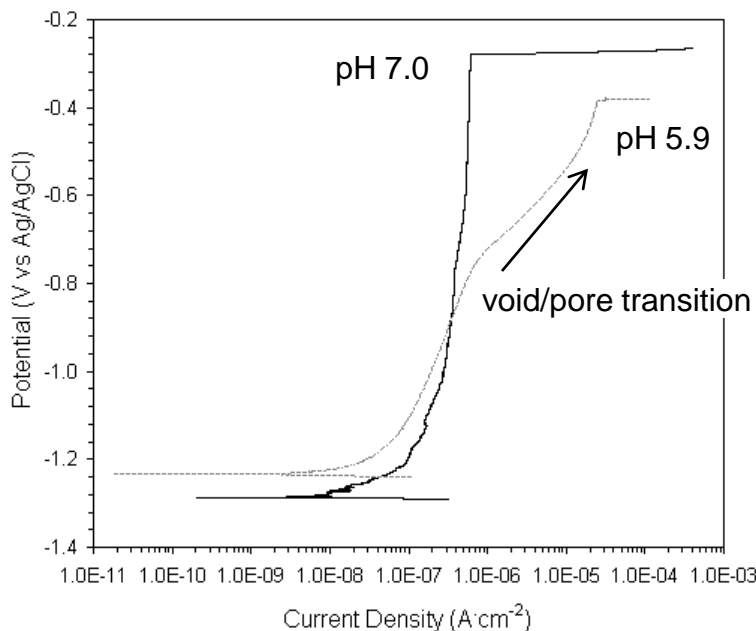
Aggressive anion and electric field perturbation - Okada



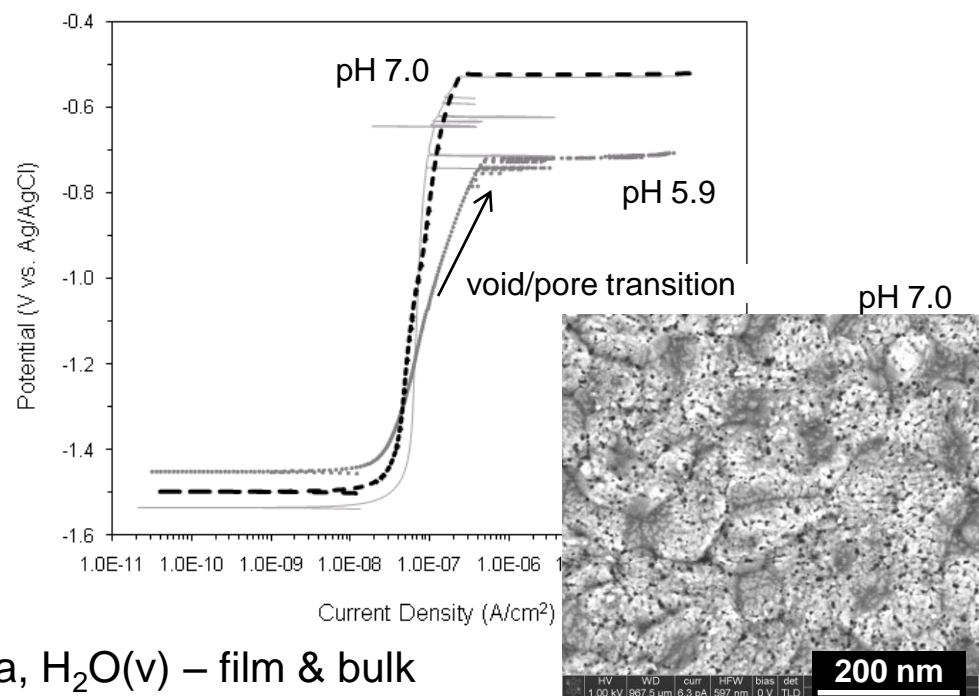
Pit initiation in model oxides on Al coincides with oxide defect activity

~150 nm diameter grain Al(111) film in de-aerated 50 mM NaCl

Macroscale measurements at 1 cm^2



Mesoscale capillary measurements at $< 0.01 \text{ cm}^2$

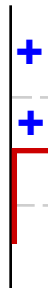


Initially anhydrous oxides – O_2 , O plasma, $\text{H}_2\text{O}(\text{v})$ – film & bulk including single crystal

I/V response shows the presence of a proton-activated process that leads to accentuated current generation – anodic dissolution can compete with pit initiation

Void nucleation as a means for relieving charge transport impedance

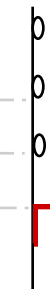
transport barrier



saturation



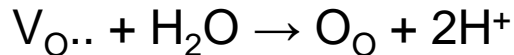
void nucleation



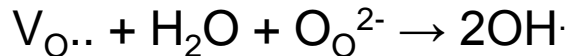
*interfacial $V_O^{i..}$. Al oxidation increases $V_O^{..}$

barrier relieved

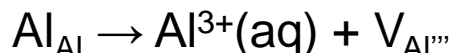
$V_O^{..}$ saturation through a simple equilibrium:



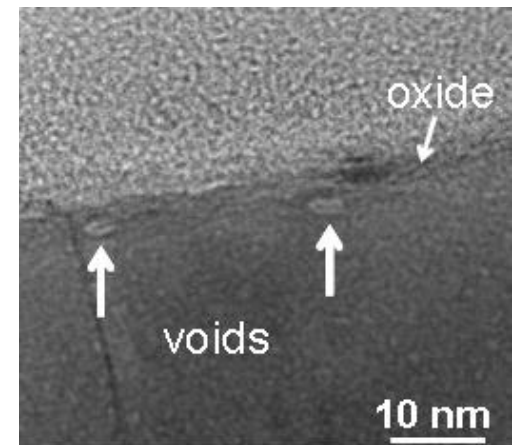
Alternate reaction to consider:



Ox:El interface barriers:



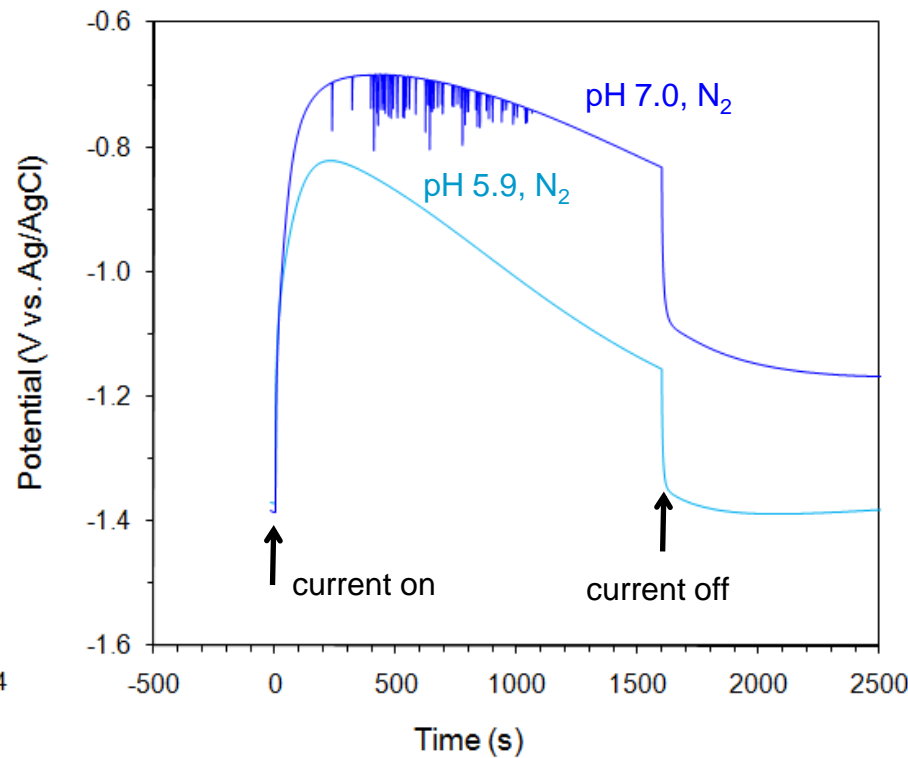
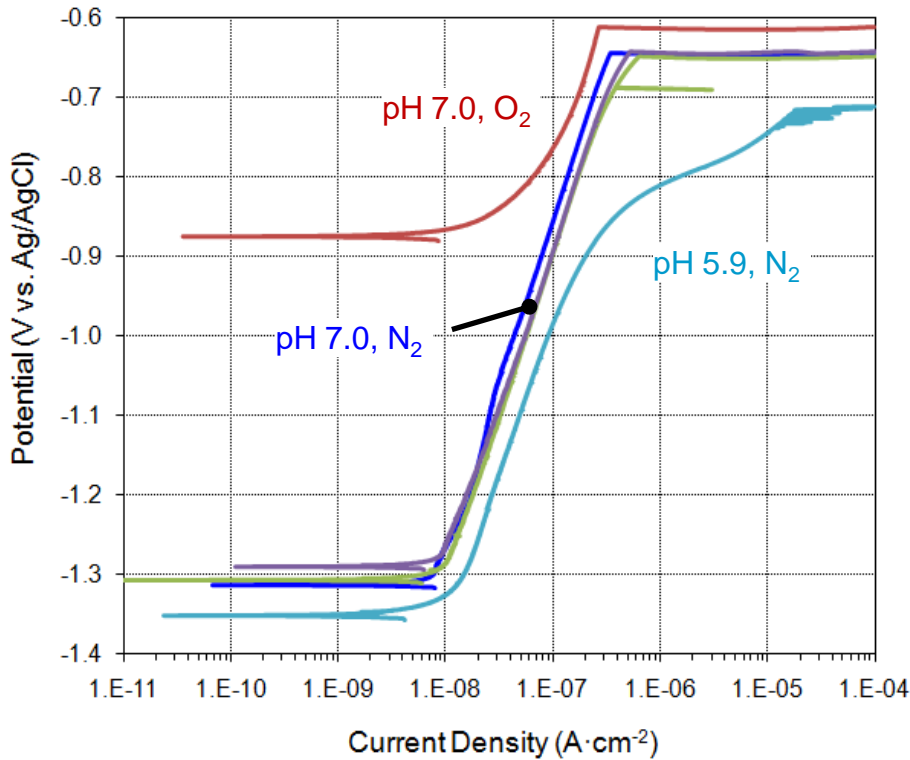
retarded by surface adsorbates or chelating species



Can imaging help determine how voids contribute to pit initiation?

Chronopotentiometry highlights the co-incidence of pitting & defect activity

700 nm thick Al(111) film in de-aerated 50 mM NaCl

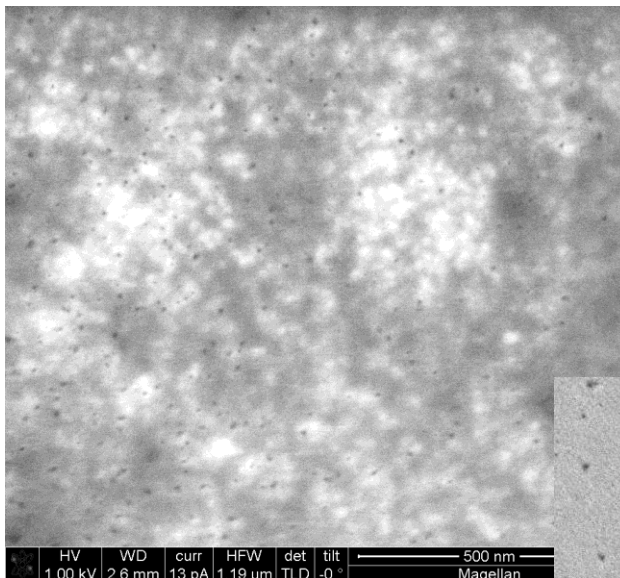
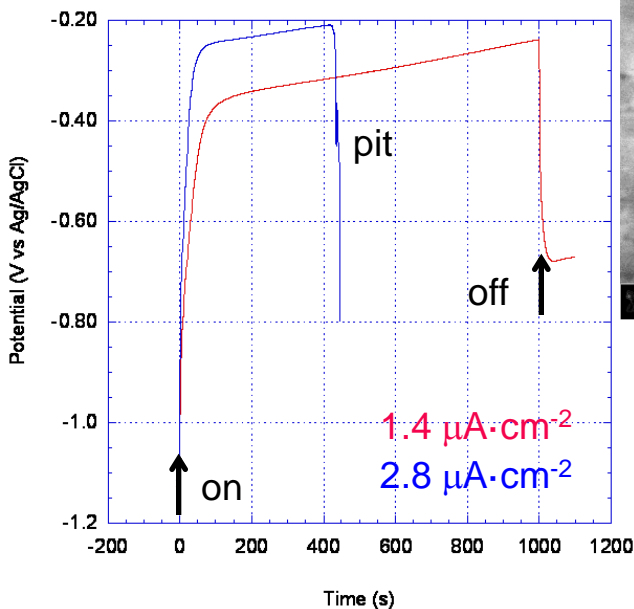


Pitting and accentuated dissolution compete

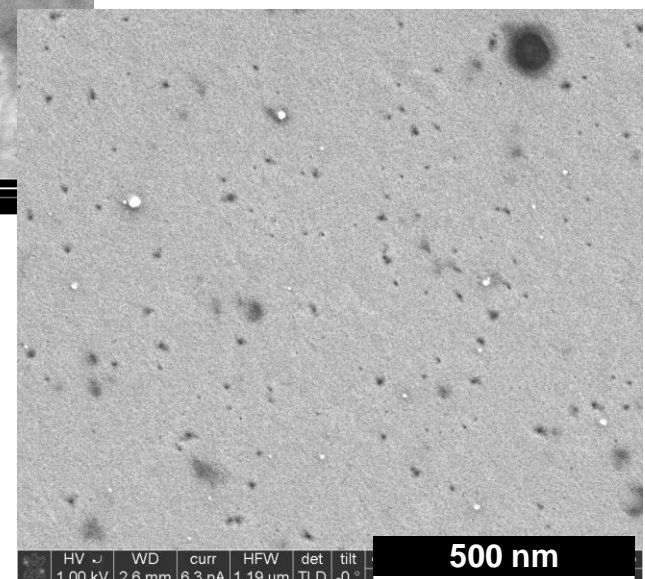
Similar defect processes operative in *not* so *model* oxides

99.999% polycrystalline Al aqueous alumina (30 nm polish) – oxide allowed to dry

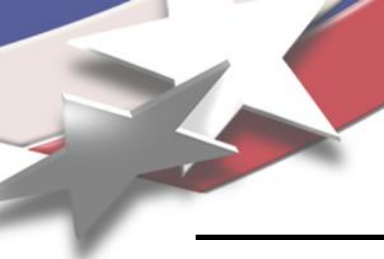
equilibrated 1 hour 50 mM Cl⁻



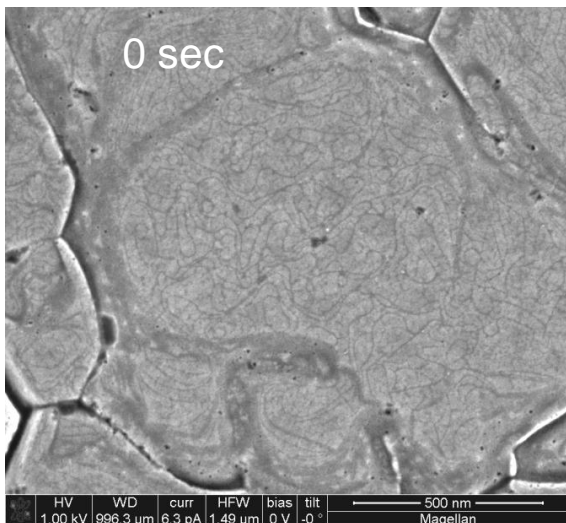
1.4 $\mu\text{A}\cdot\text{cm}^{-2}$, 1.4 mC



Model oxides may represent one way of probing the limiting cases of defect chemistry



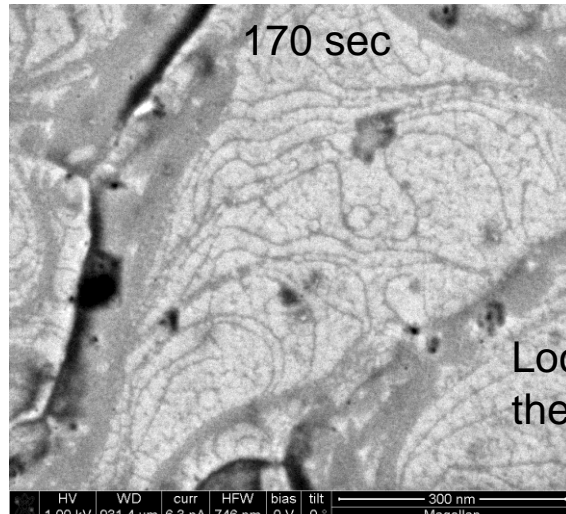
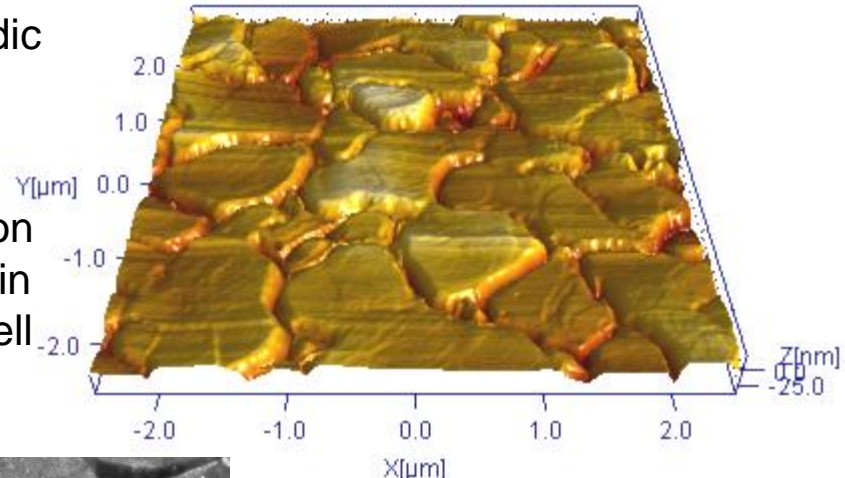
Structural impact of polarization is greatest at the high step density facets of the grains



700 nm thick Al(111) film in de-aerated 50 mM NaCl pH 7
– larger grains for better spatial discrimination

0.6 μ A·cm⁻² anodic polarization for variable time

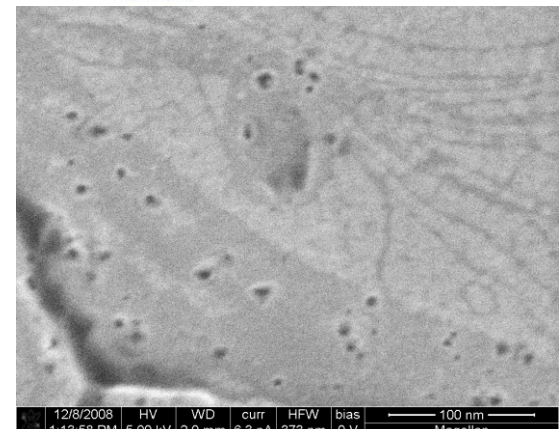
void/pores form on contours into grain boundaries as well as terraces



1600 sec with pitting
Possible pit covered with oxide

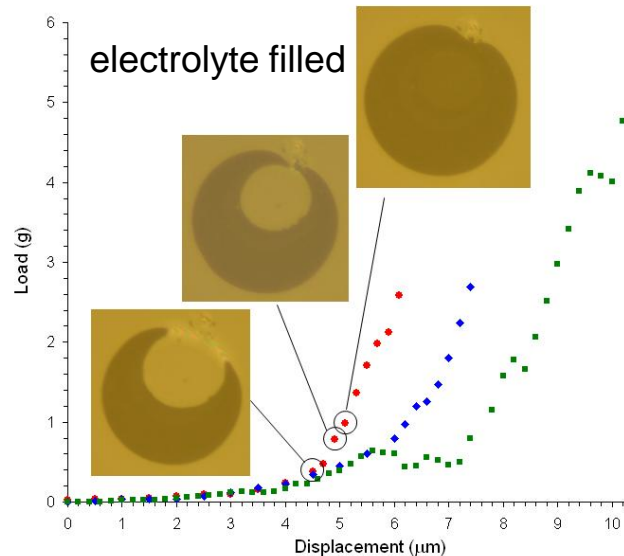
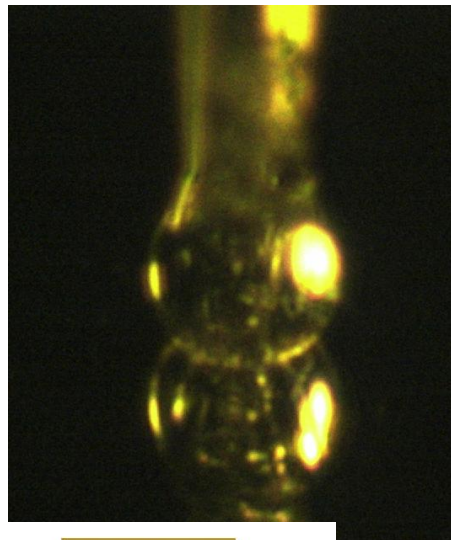
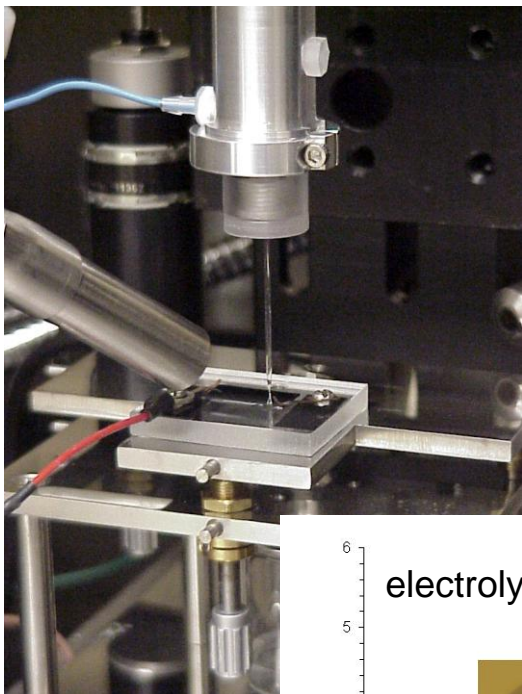
Local dissolution at the terrace surface

HV 1.00 kV WD 994.7 μm curr 6.3 pA HFW 1.49 μm bias 0 V tilt -0° — 500 nm —
Magellan

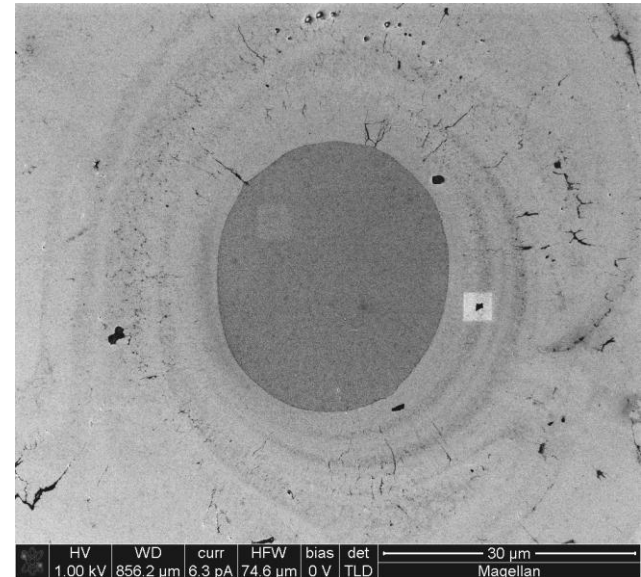




Can more detail be learned by restricting area to enable imaging?



Snapshot approach

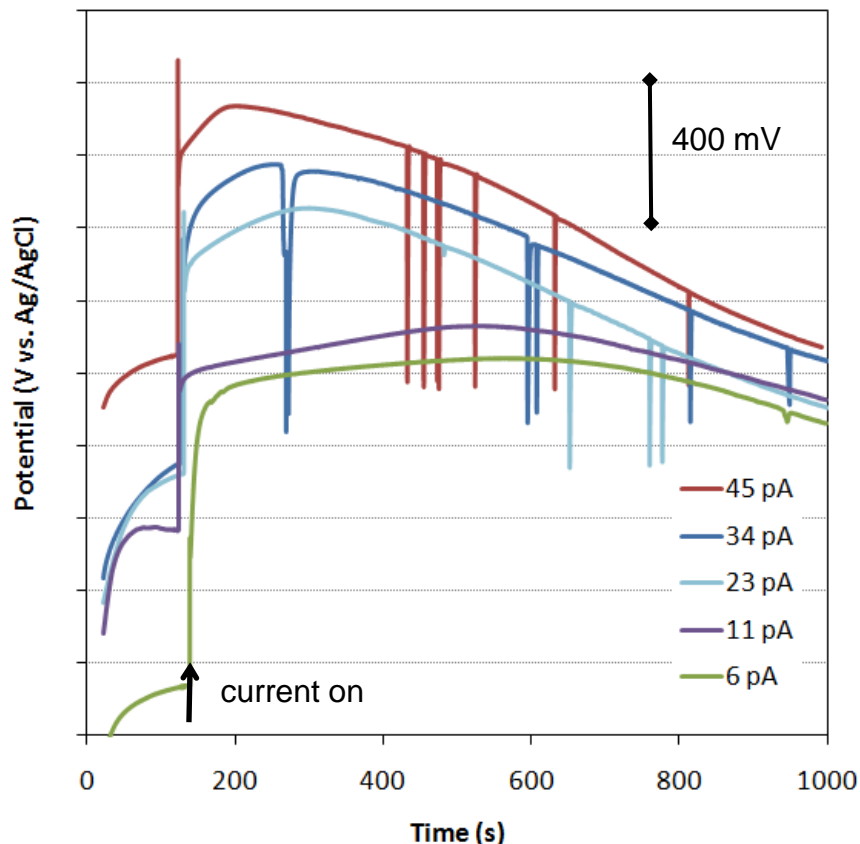


Size limits – leak free seals with minimal under seal activity at 20 μm diameter, $1 \times 10^{-6} \text{ cm}^2$

Current limits – galvanostatic polarization at relevant current densities

Defect and breakdown signatures are measureable in the micro-cell

Anodic polarization using a 20 μm diameter capillary



i (pA)	j ($\mu\text{A}\cdot\text{cm}^{-2}$)	t_{\max} (s)	E_{\max}^* (mV)	events
45	15	73	45	multiple, frequent
34	11	125	-38	multiple, frequent
23	7	320	-82	multiple, infrequent
11	4	480	-172	multiple, infrequent
6	2	450	-159	single, rarely
3	1	1930	-252	none detected

*vs. Ag/AgCl

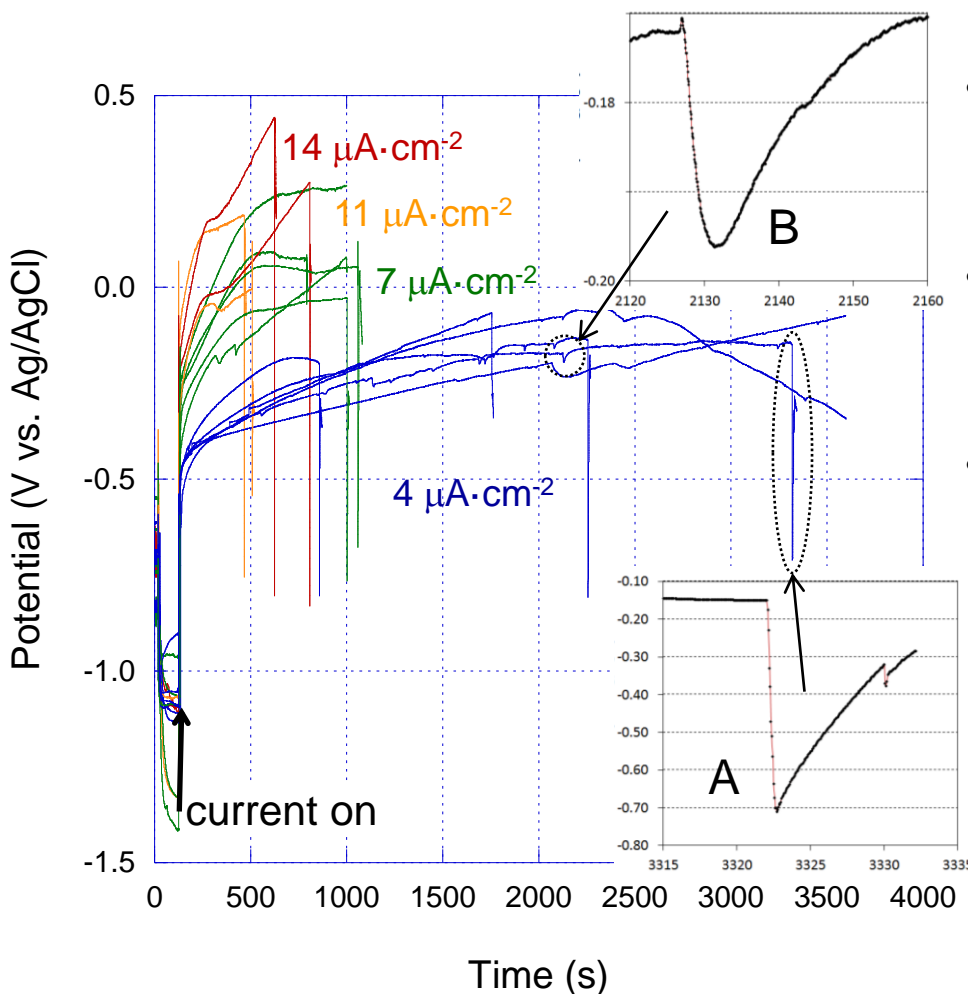
Defect response is observed with anodic polarization

Breakdown events are observed at potentials > -550 mV vs. Ag/AgCl

Likelihood of a breakdown event scales with current magnitude

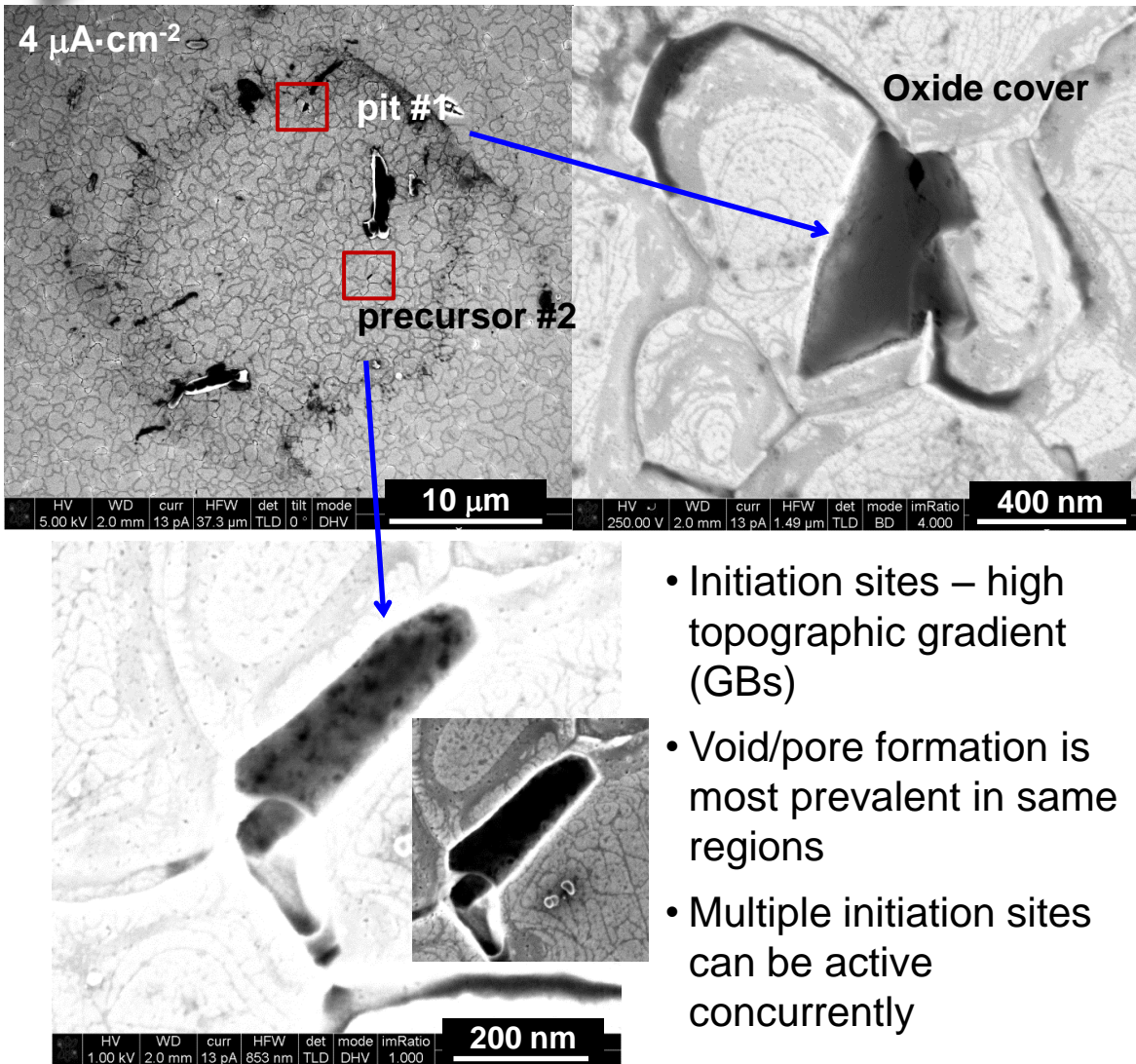
Drive single breakdown events – characterize the event signature – correlate events with evolved surface structure

Attributes of Single Discharge Event Experiments



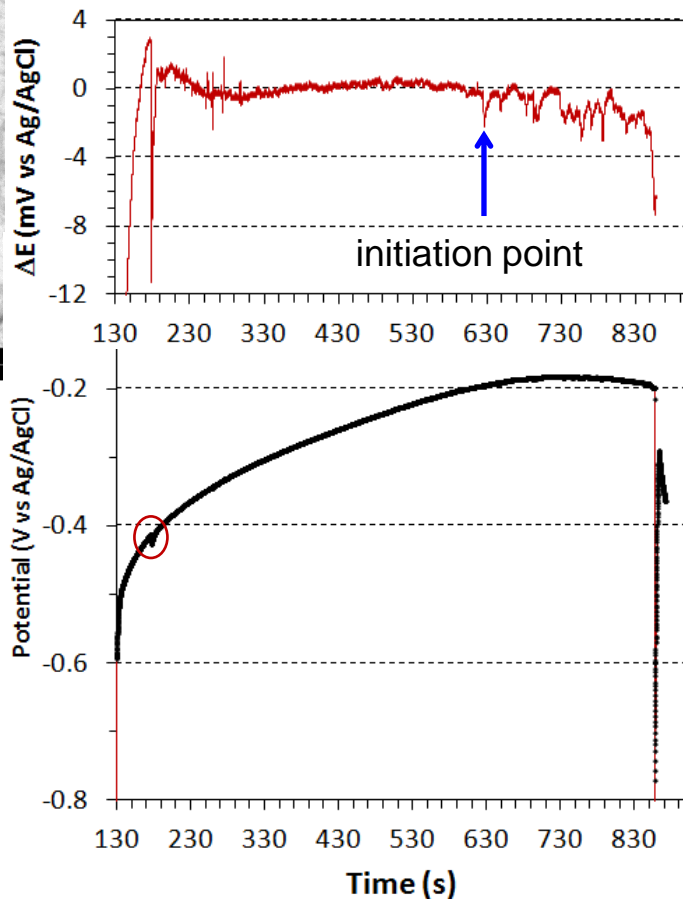
- Increased applied current density – higher probability of creating an event
- increased applied current density - shorter induction time for event occurrence
- Two types of depolarization signatures
 - large magnitude discharge events (A)
 - small magnitude or extended time perturbations (B)

Sufficient current becomes localized to drive early stage pit formation

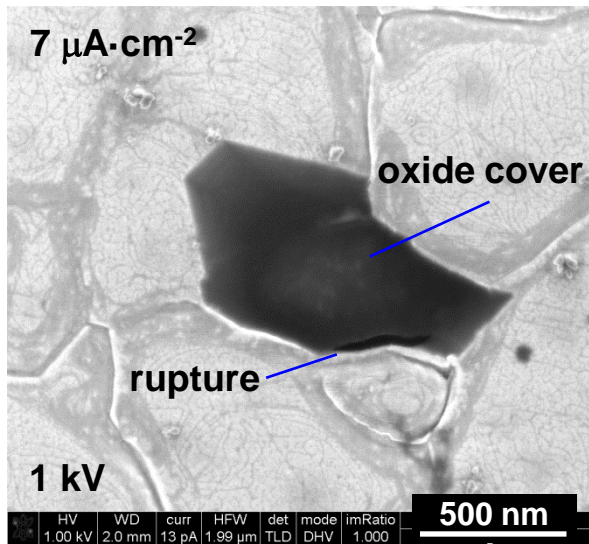


- Initiation sites – high topographic gradient (GBs)
- Void/pore formation is most prevalent in same regions
- Multiple initiation sites can be active concurrently

- Initiation signature appears to be the small $\delta E/\delta t$ fluctuations

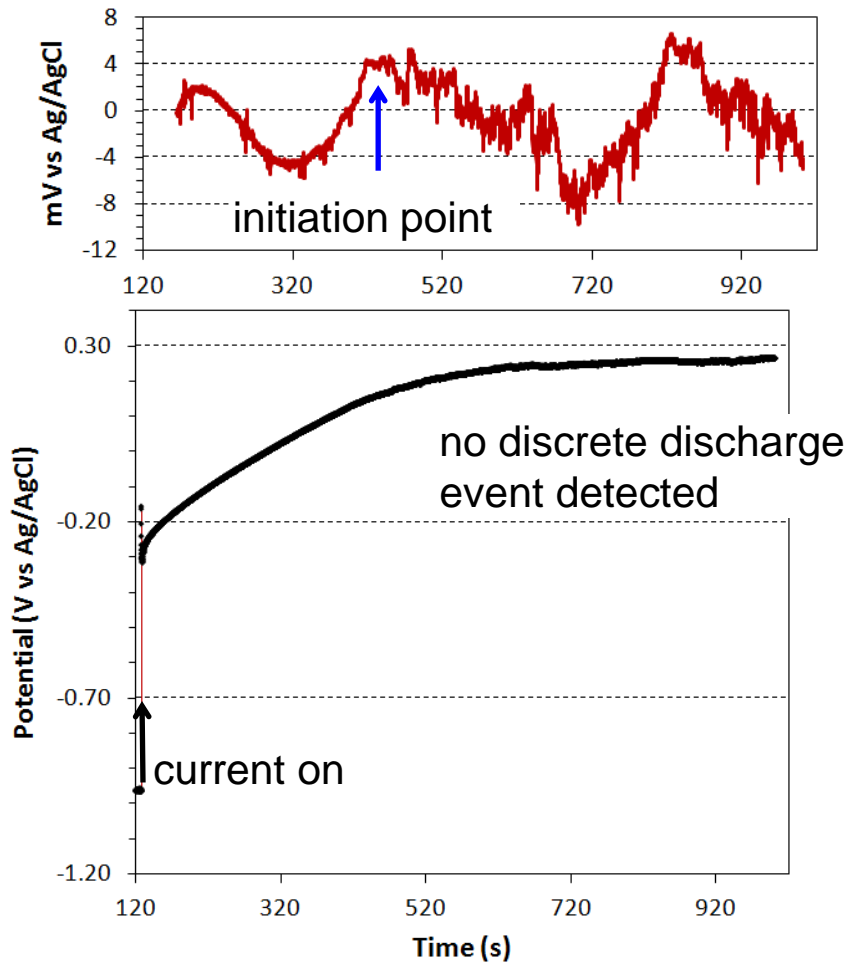


Electrochemical noise may also signal slow growth of an early stage pit

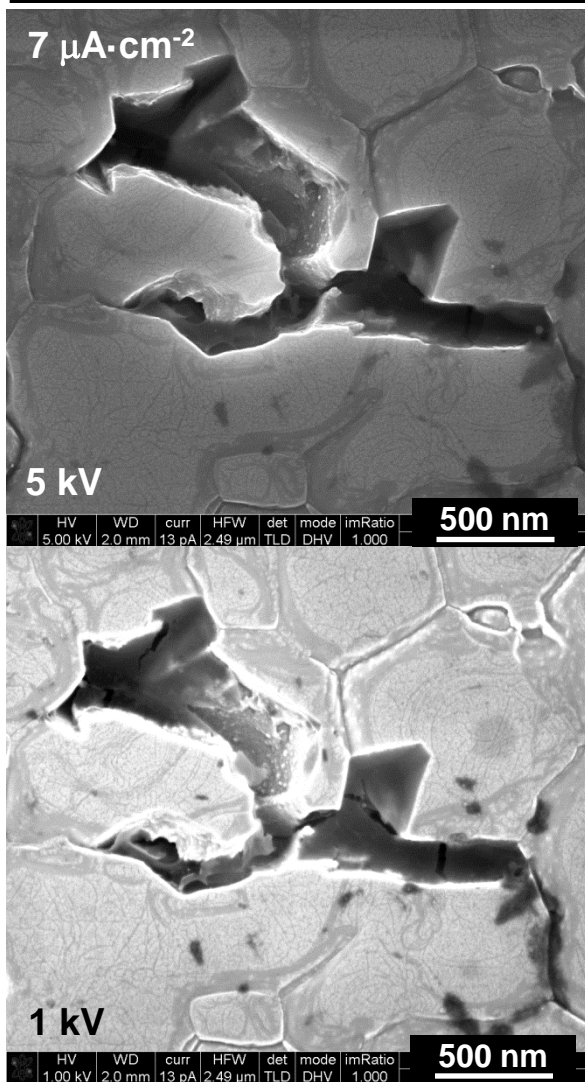


An occluded pit is observed despite the absence of a significant magnitude discharge event

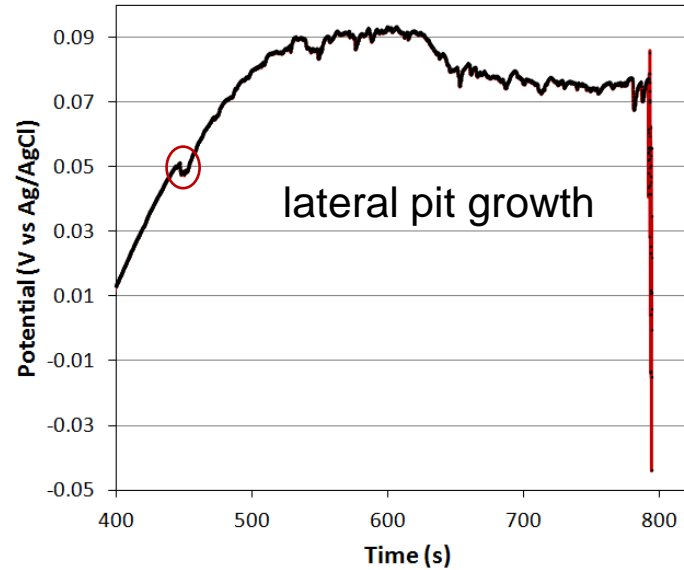
- EC noise is a better indicator of micro-cell activity



Extended lateral growth of a pit complex can exhibit a similar low amplitude signature



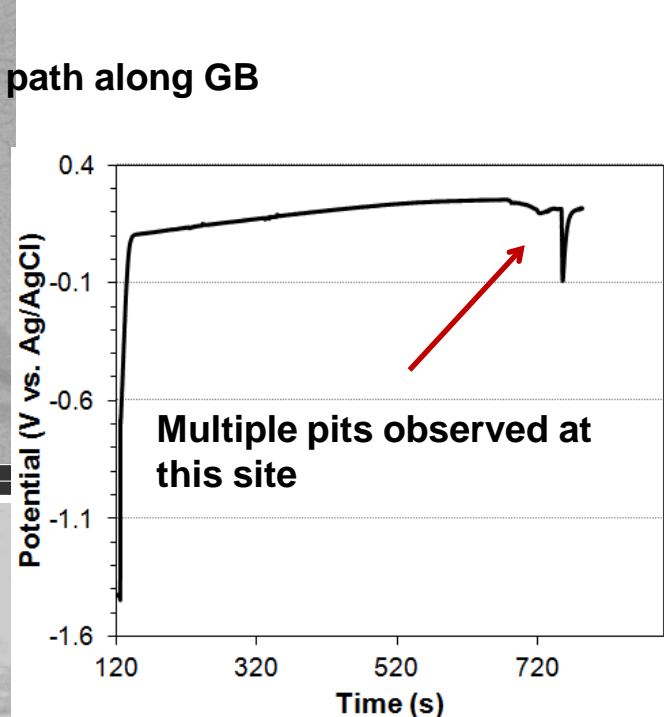
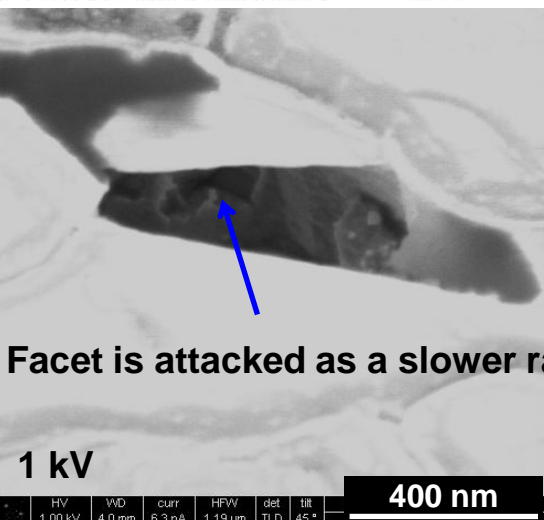
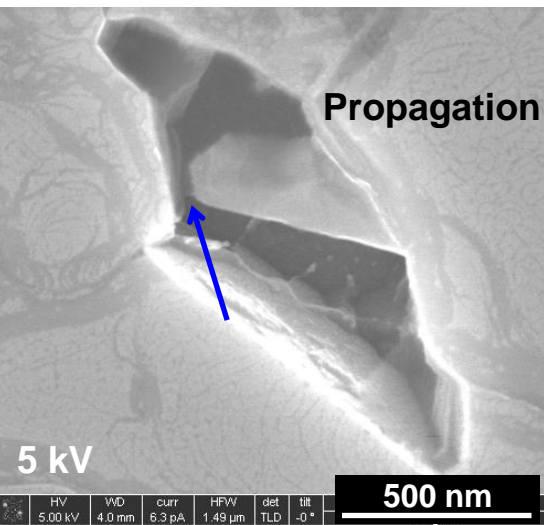
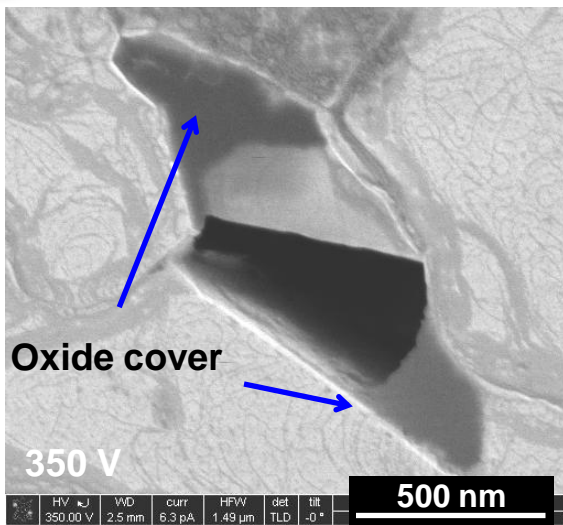
Single active area detected for this experiment



Lateral propagation favored by several factors

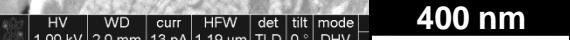
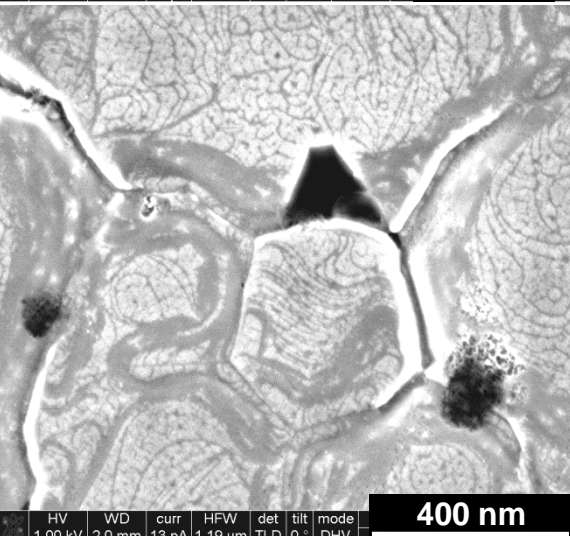
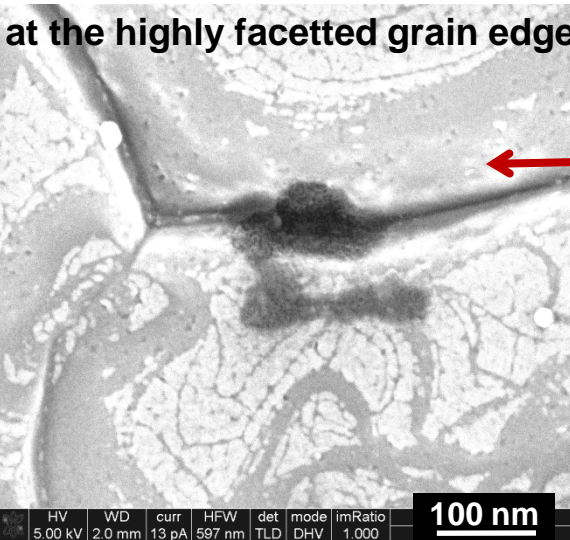
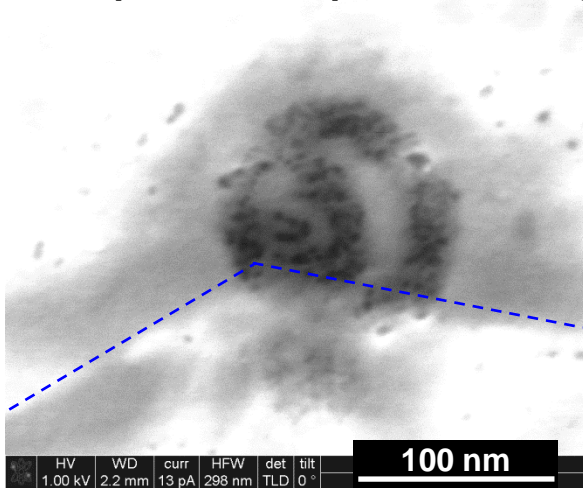
- (111) texture – favored dissolution planes are in-plane
- Grain boundary as a short circuit

Staged pit growth aided by a grain boundary and compliant oxide cover



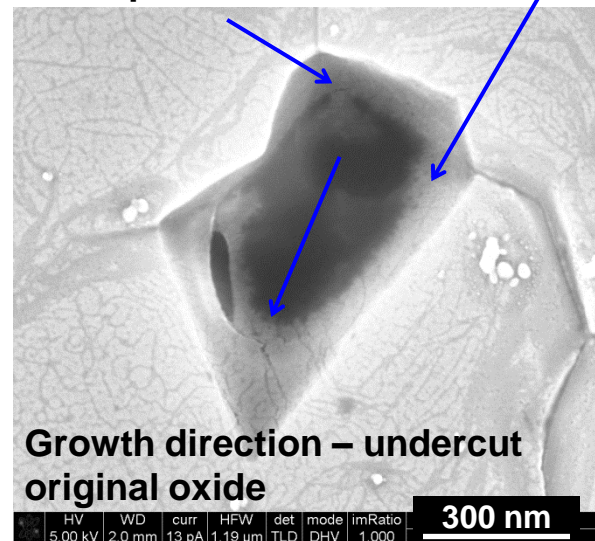
Evidence exists for interfacial voids acting as initiation sites

Examples of void/pore clustering at the highly faceted grain edge



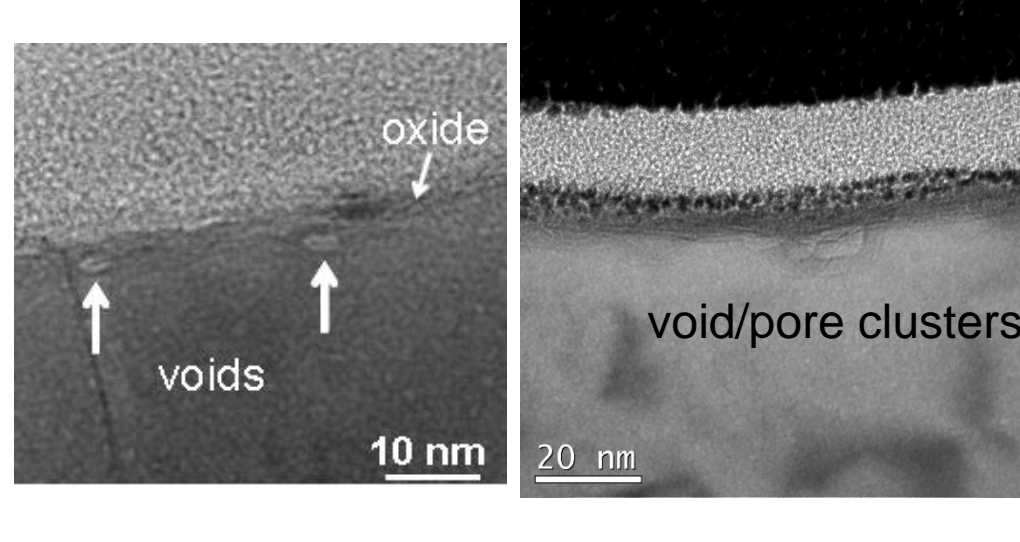
These initiation structures are seen in evolving pit structures

Pore perforated initiation site

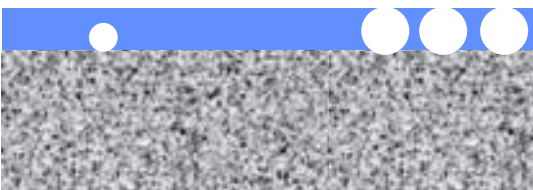


Interfacial voids as pit precursors

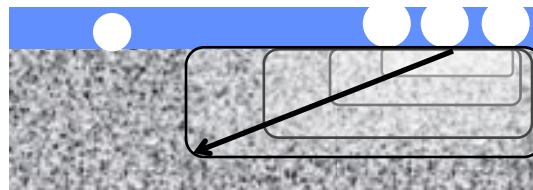
Void nucleation



Growth and pore formation



Stable cluster formation – oxide perforation



Pit nucleation under oxide membrane

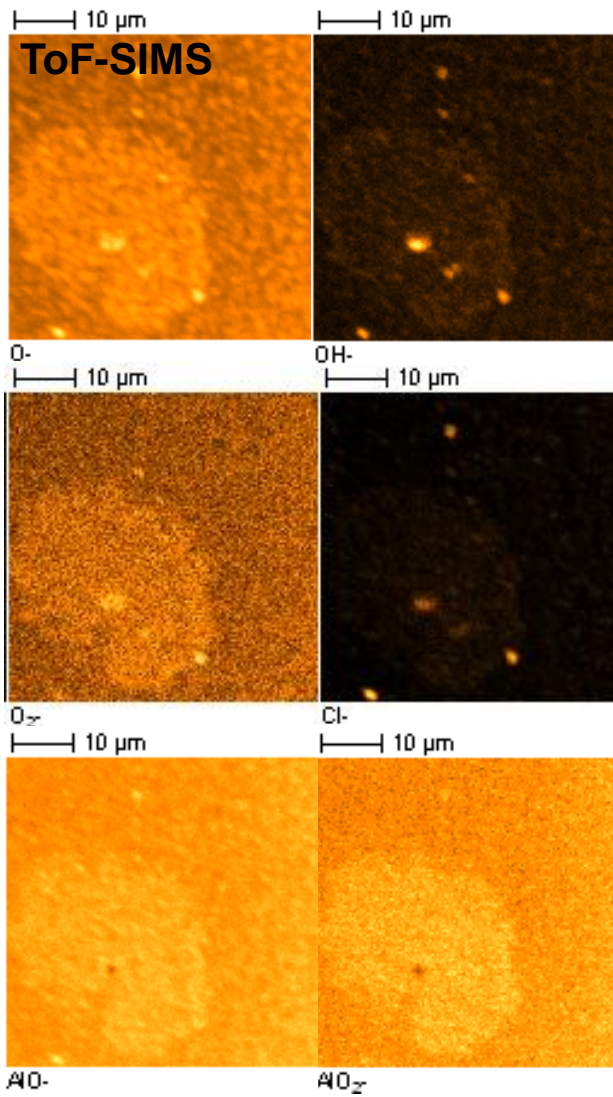
High gradient topology as the nucleation region:

Greatest local flux of Al cations

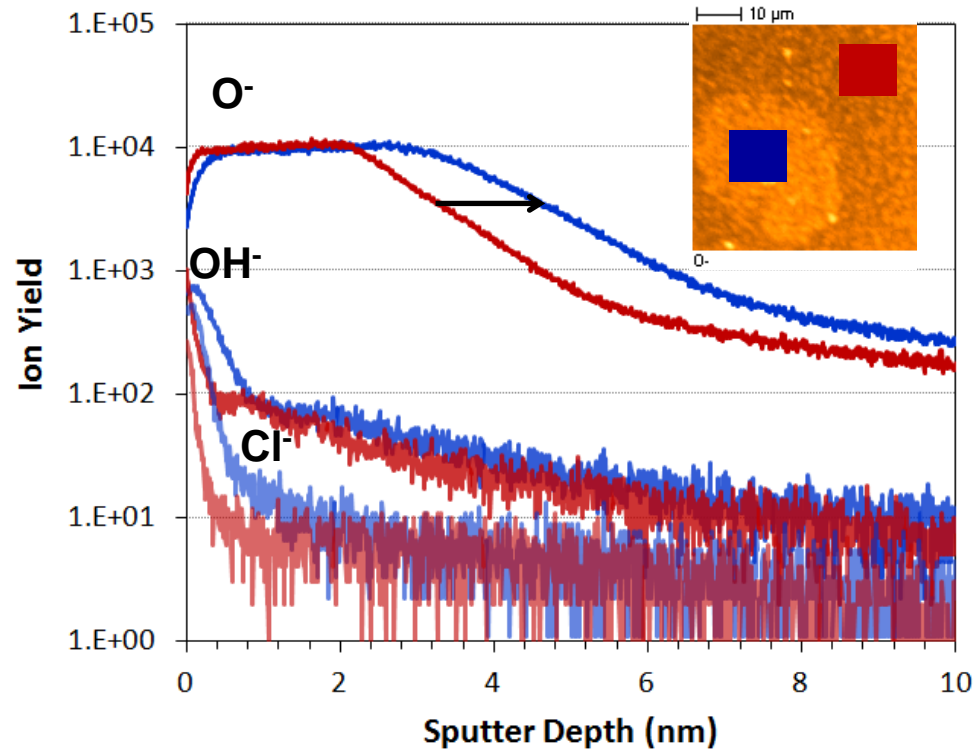
Structurally strained oxide

Steps stabilize void nucleation

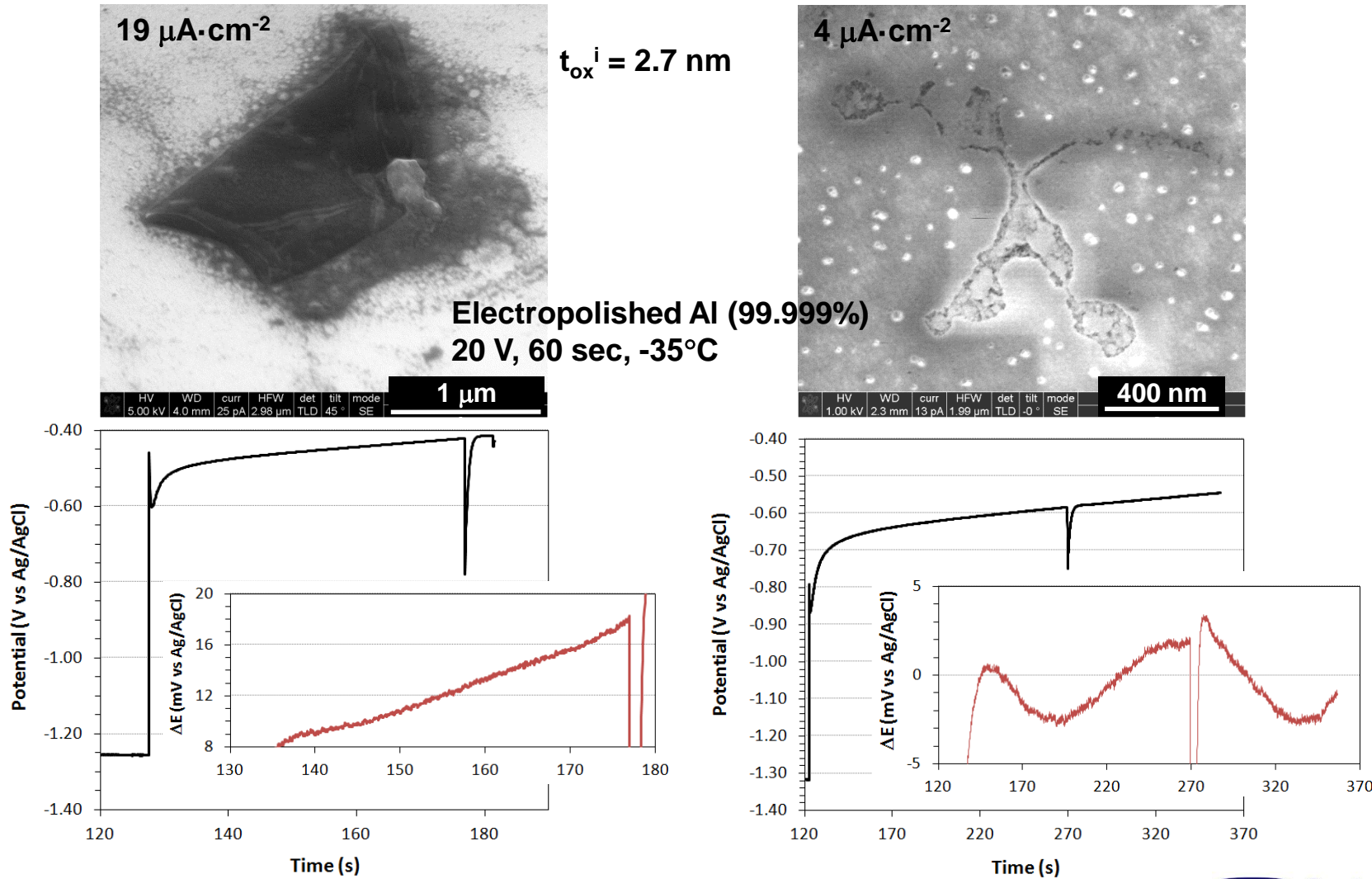
Polarization drives oxide growth with minimal compositional change to the film

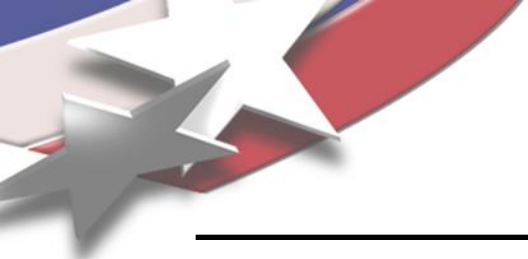


- Oxide growth: 10% from electrolyte immersion, 20 to 40% with polarization
- Cl⁻ primarily restricted to the hydrated outer layer



The lower impedance of a hydrous oxide requires higher currents to yield pits





Conclusions

- Restriction of electrode size and controlled galvanostatic polarization can be used to drive and characterize single breakdown events
- Breakdown produces structures ranging from undercut membranes to oxide capped early stage pits
- Pits initiate predominantly at the highly stepped perimeters of the grain boundaries – regions demonstrated to be active void and pore nucleation sites
- Void/pore structure is observed in evolved pits arguing that void nucleation serves as the precursor event for pit initiation in aluminum
- Currently working to apply this demonstrated level of control in *in situ* observation of pit initiation